

Oser



Laetitia Gaultier & Frédéric Bouquet

La physique autrement



Julien Bobroff



Lou-Andréas Etienne



Frédéric Bouquet

Oser

Objectifs :

- Présenter des pratiques modernes ;
- Ateliers pratiques de science frugale ;
- Tester et développer des activités.

Culture scientifique expérimentale


En pratique :


- 14h30 à 16h30 ou 17h00 ;
- Dates : 09/11, 23/11, 07/12, 04/01, 18/01, 01/02, 15/02 ;
- Institut Villebon Georges Charpak ;
- Présentation, puis atelier ;
- Peu de travail en dehors ;
- Ateliers tests les quatre premières séances ;
- Projet les trois dernières séances.


Les grands Instruments


Google les grands instruments


vent guitare cuivres livre scientifiques caractérisation grenoble trompette train



grand livre des instrum...
librairie-gallimard.com · L...



musique "Beaux Livres ..."
chroniquesdemadoka.ekl...

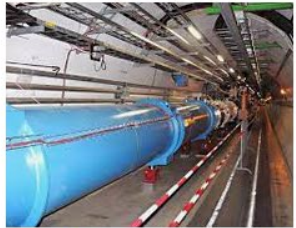

de musique ...
musiclic.com



Très grands instruments - Institut Neel
neel.cnrs.fr



musique à cordes - Violon Alto
violon-alto.fr



Quel est le plus grand instrument de ...
digital.playbackpresse.fr



Les Instruments Avec Le G...
fr.dreamstime.com



6 grands instruments scientifiques qui...
franceculture.fr

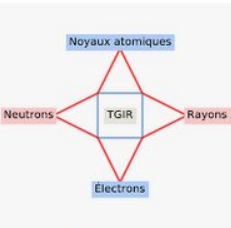

Grand Instrument de musiq...
cdiscout.com



Très grands instruments - Institut Neel
neel.cnrs.fr



Musique : « Pour les artistes prendre ...
culturelink.fr


grand livre des instrum...
ledevoir.com

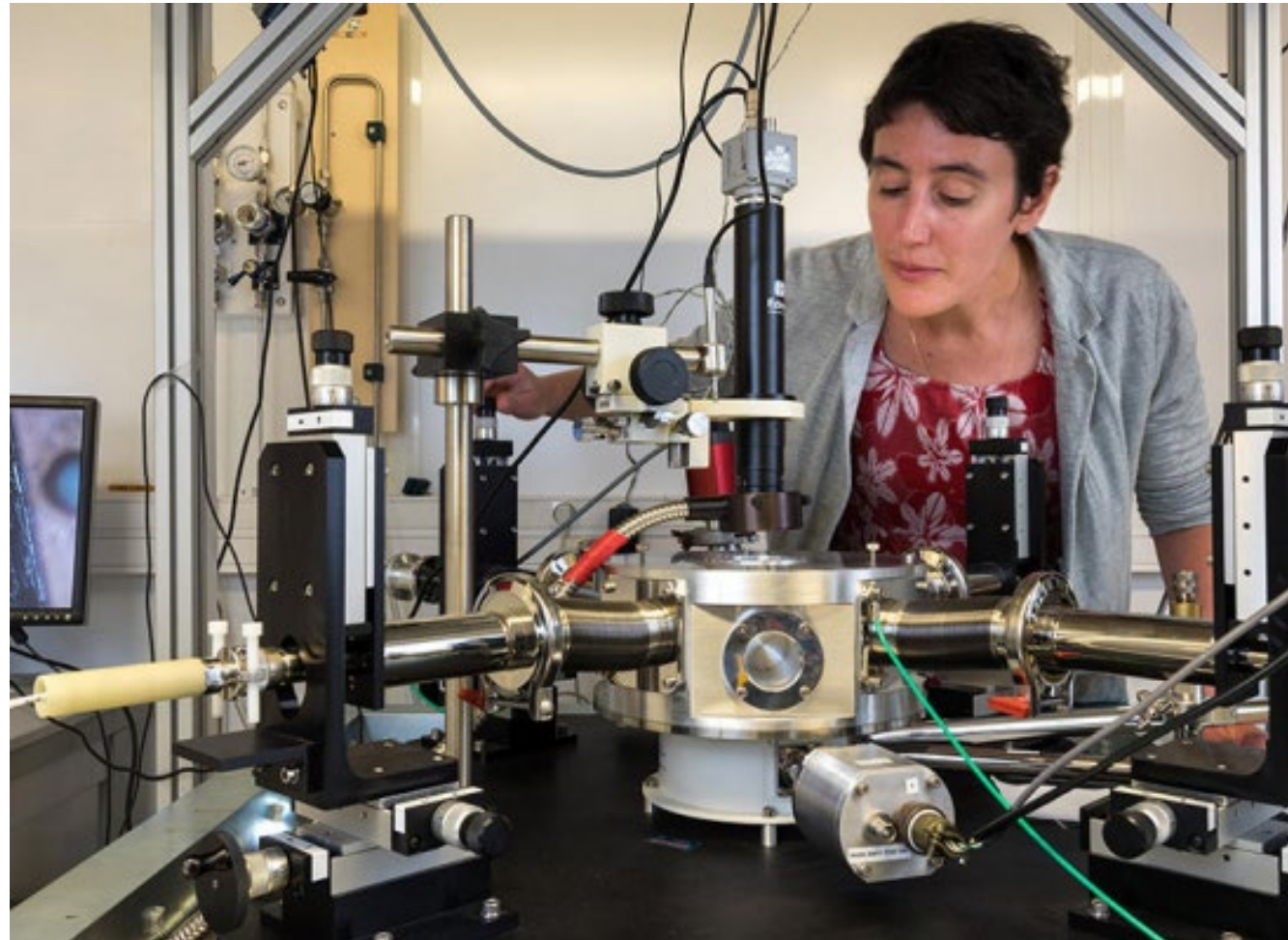

Viole de gambe. Cultur...
alamyimages.fr


Grands instruments
afc.asso.fr


magie des Instruments, les gran...
fr.shopping.rakuten.com · In stock


Instruments de musique...
gallimard-jeunesse.fr

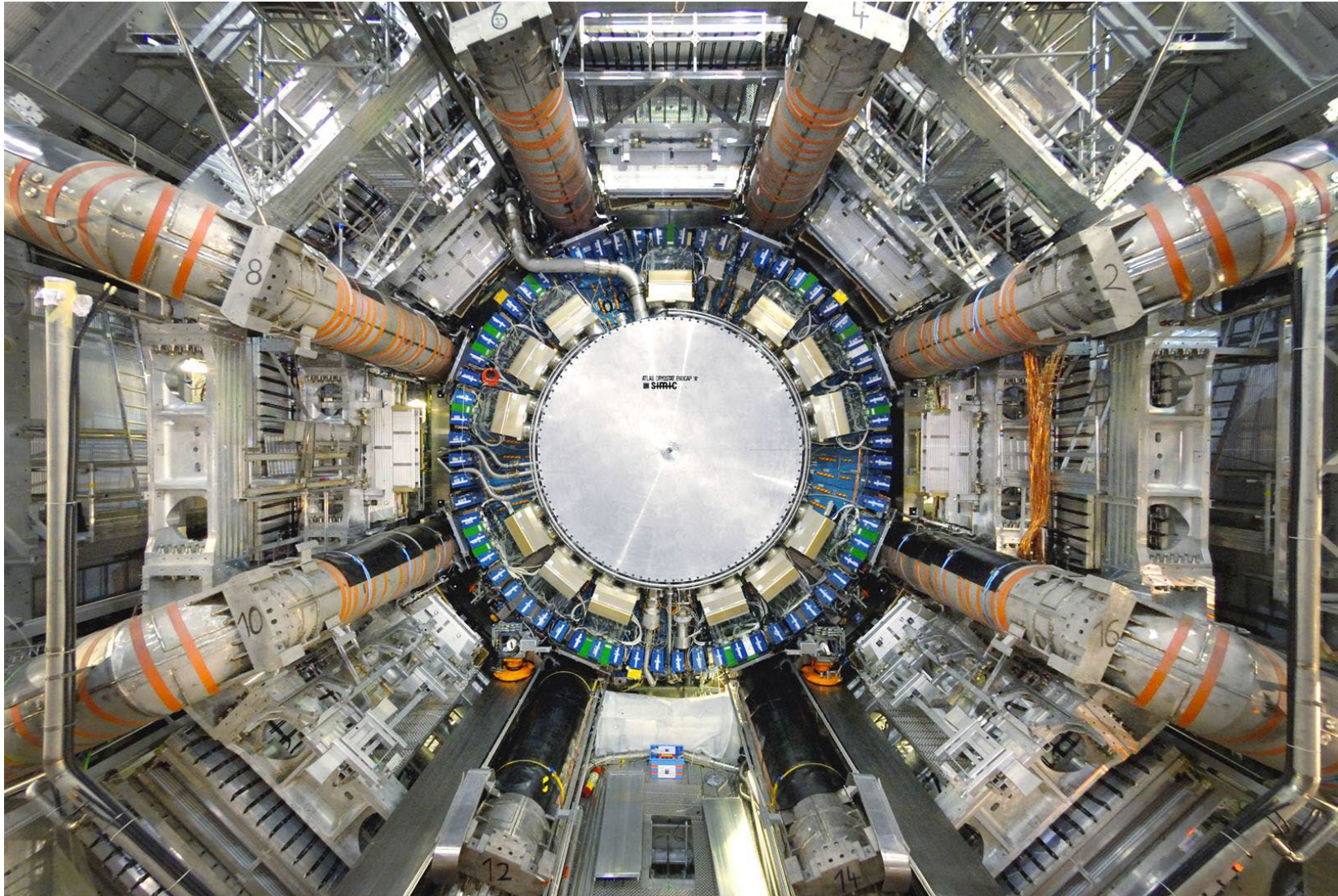
1 pièce, 1 manipe, 1 chercheur ou chercheuse

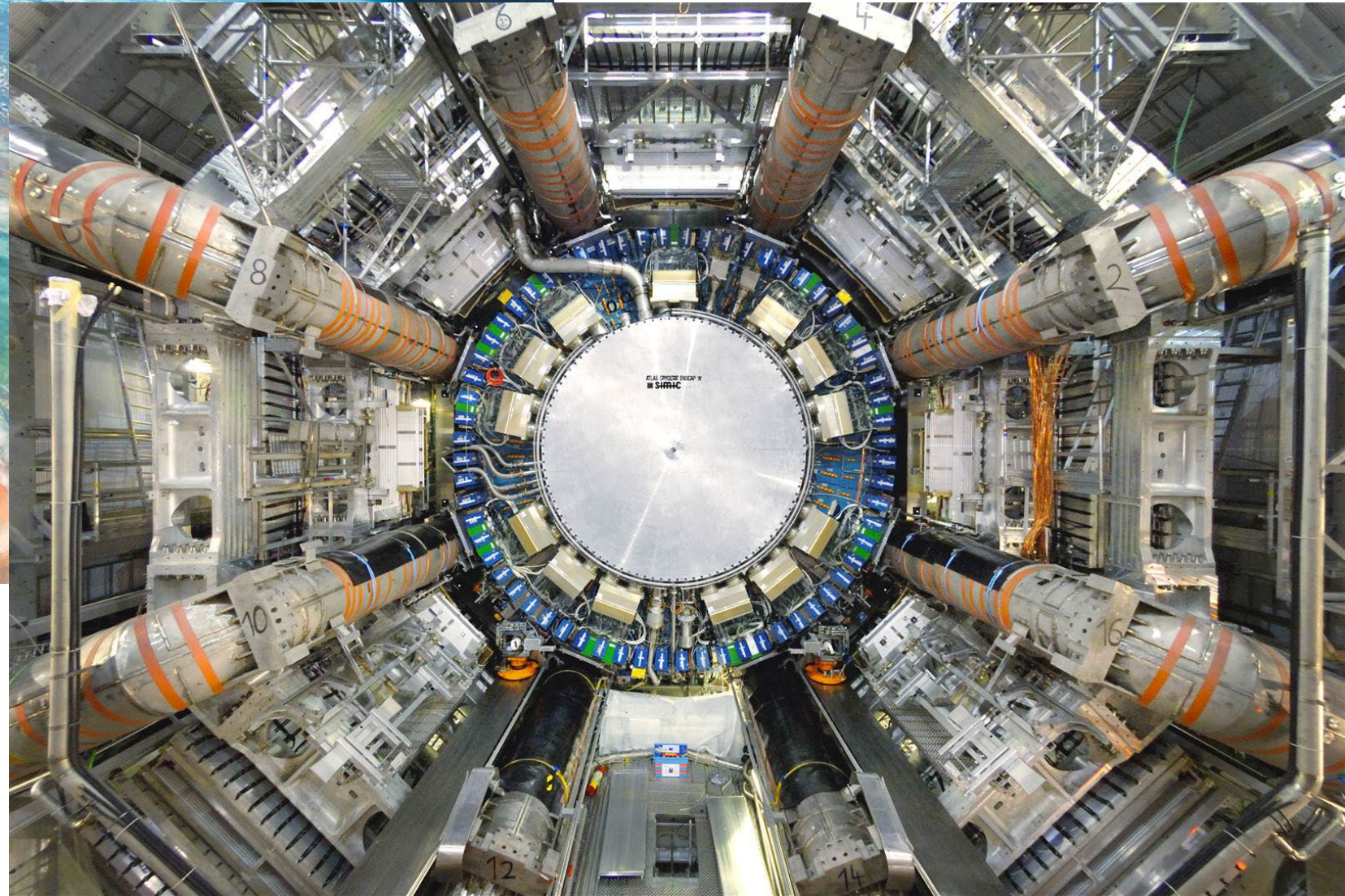


1000 pièces, 1 manipe, 1000 chercheurs ou chercheuses



1000 pièces, 1 manipe, 1000 chercheurs ou chercheuses





Les Grands Instruments



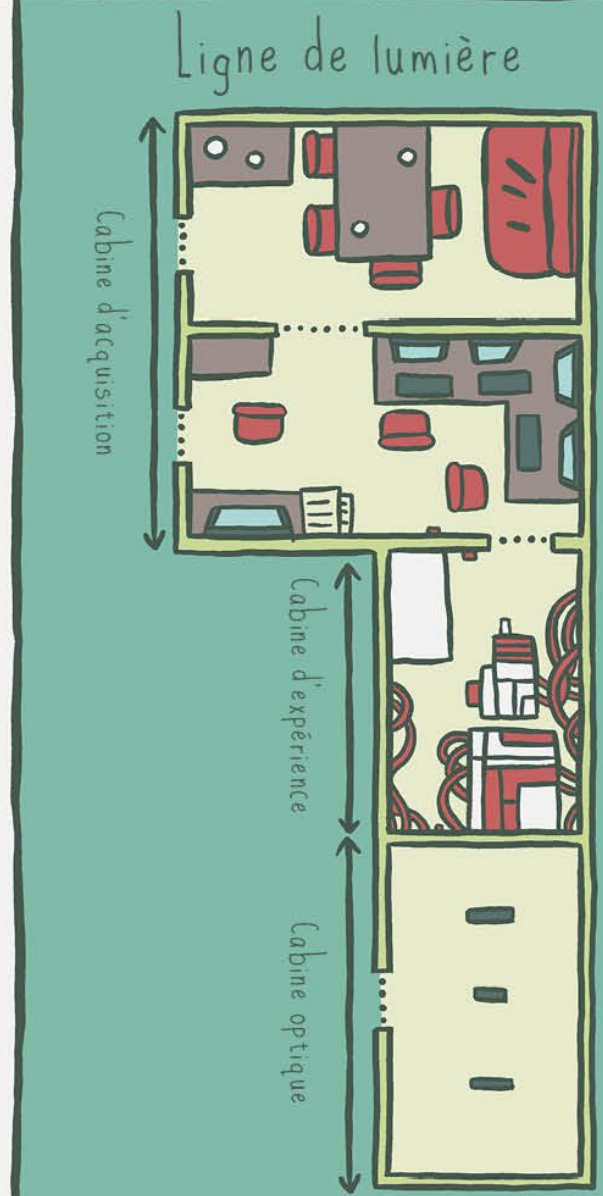
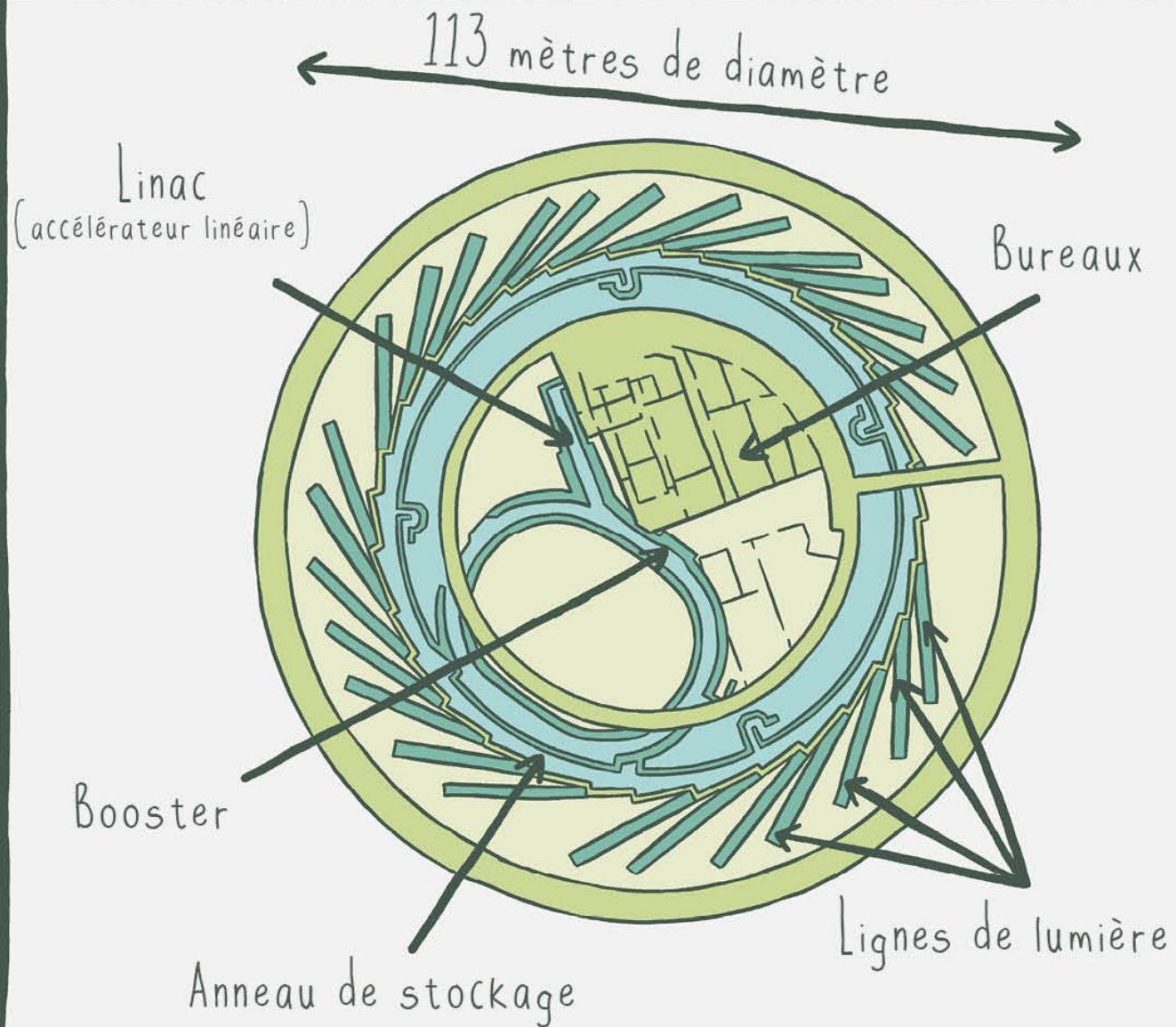




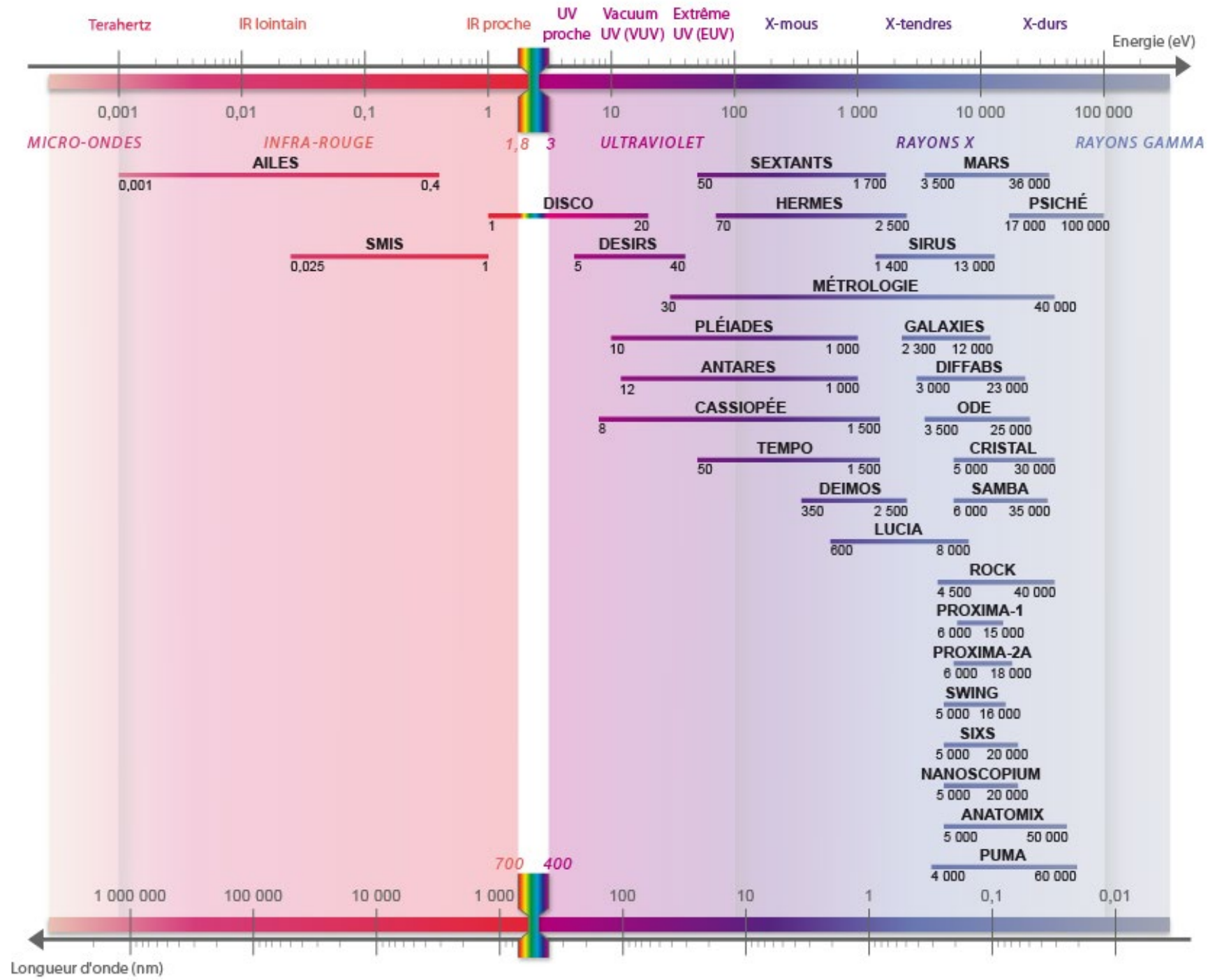
Les Grands Instruments



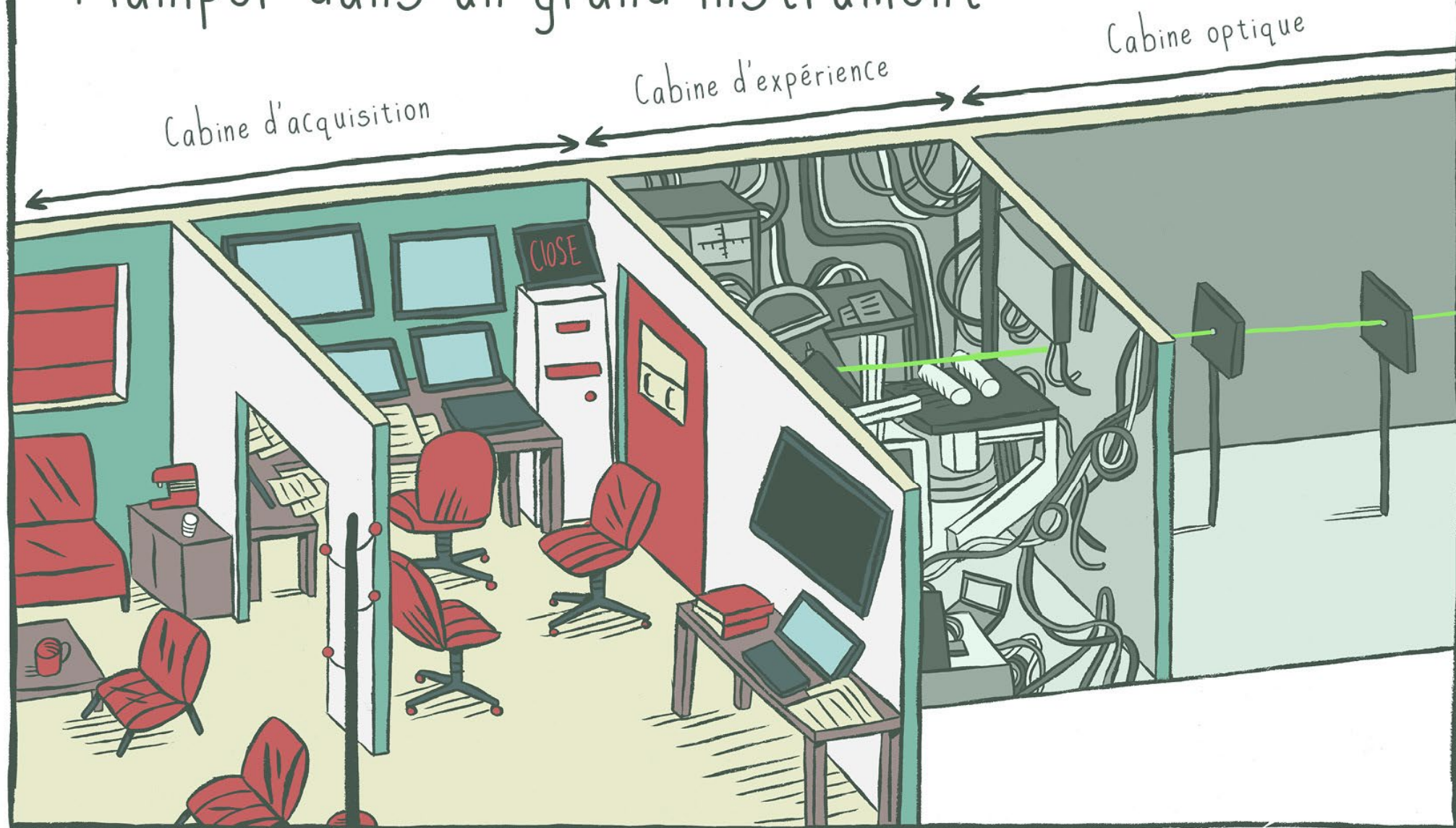
Le synchrotron

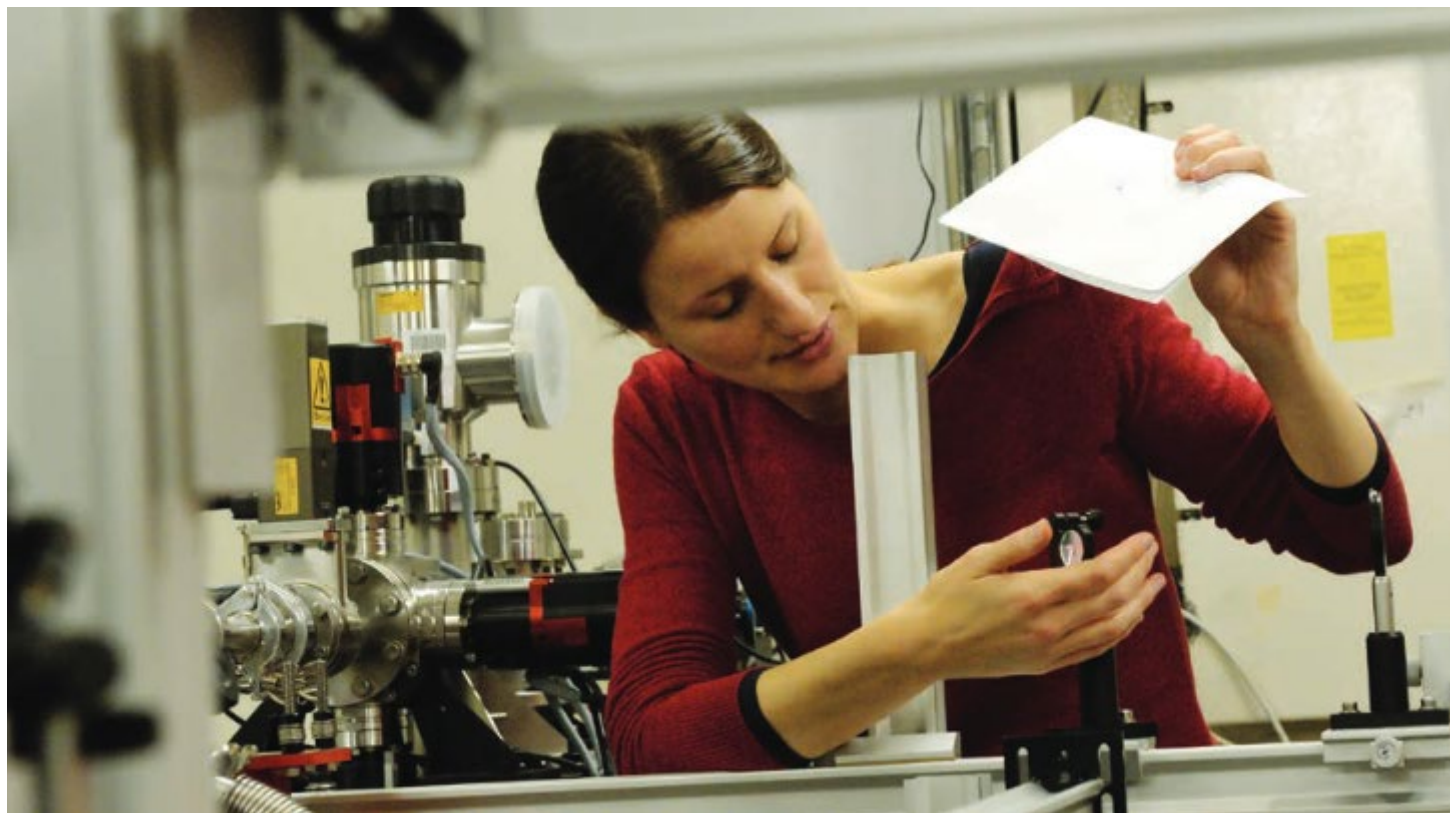


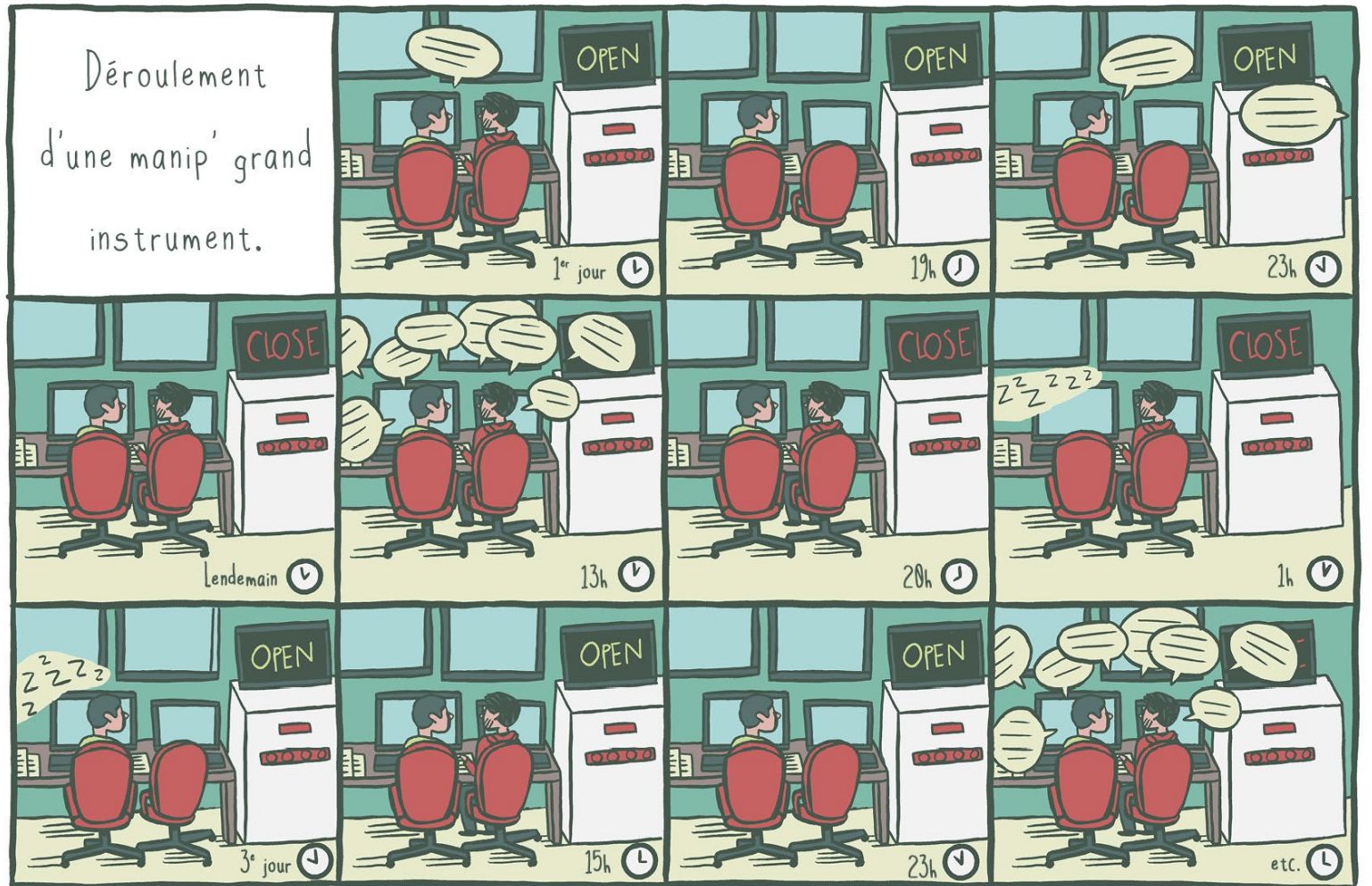


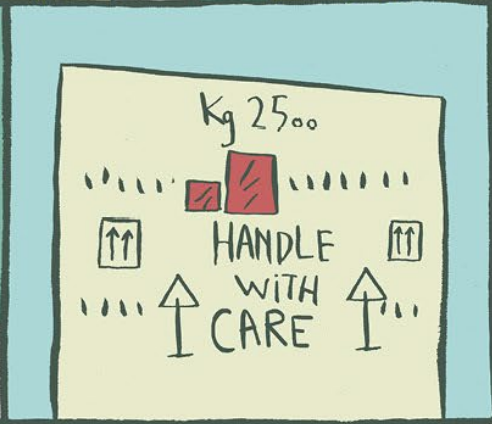
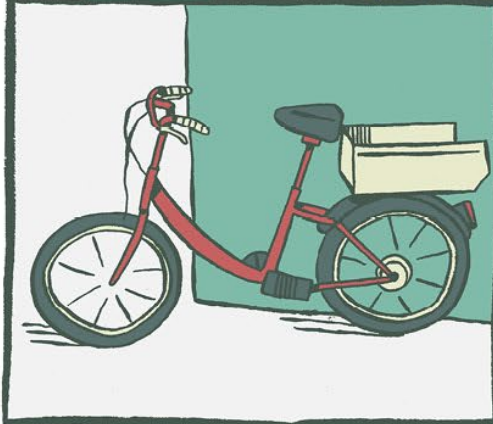
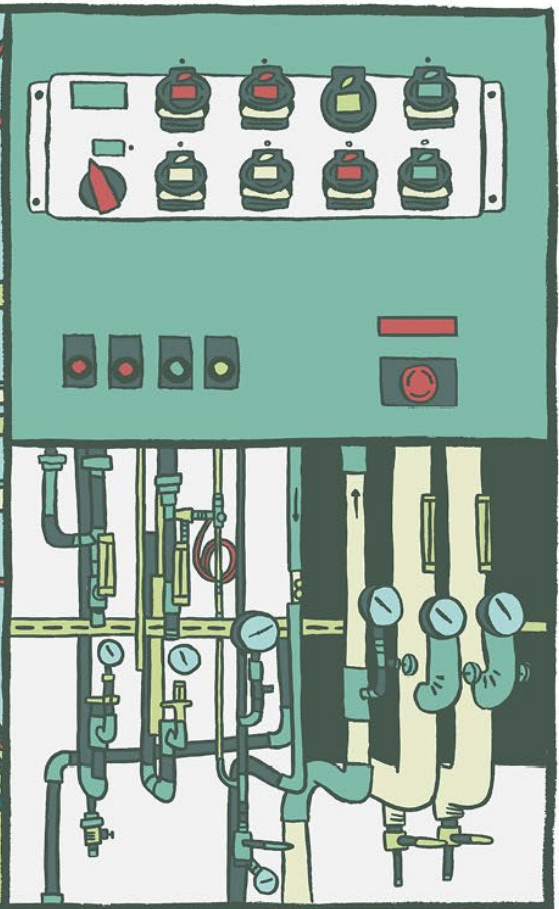
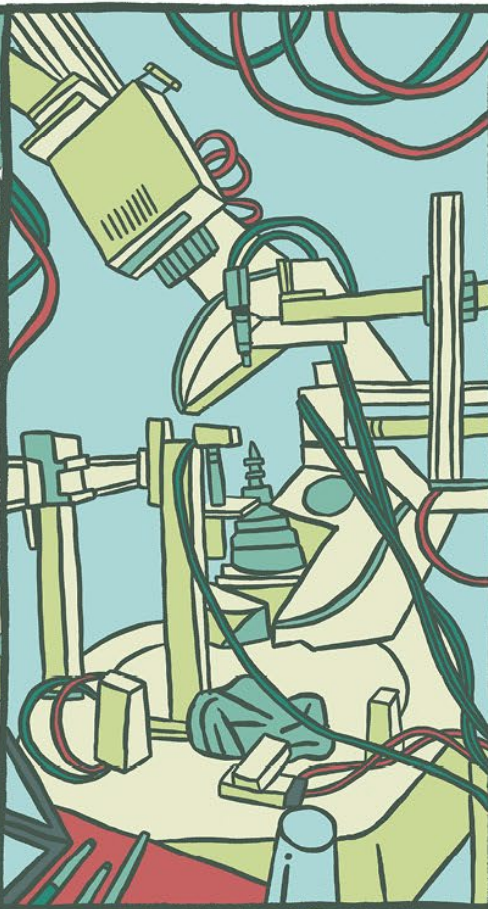
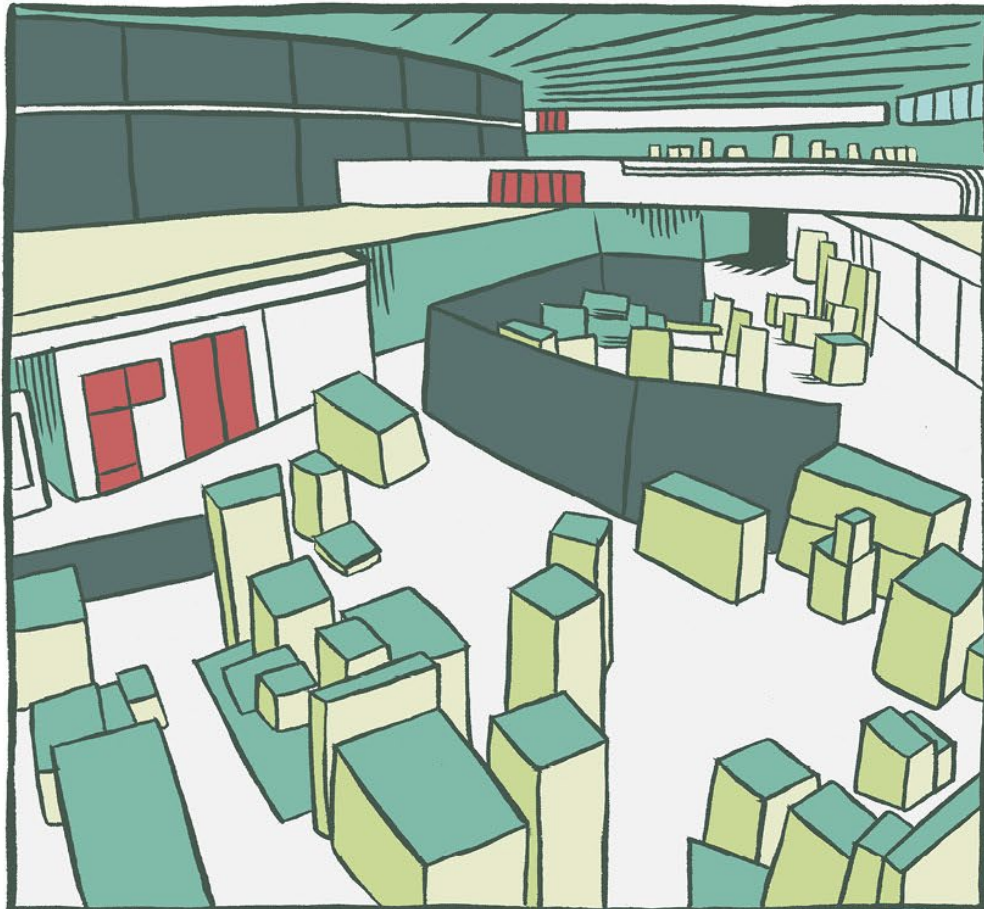


Manipuler dans un grand instrument









Interplay of spin polarization, Gilbert damping and ultrafast demagnetization in Heusler compounds

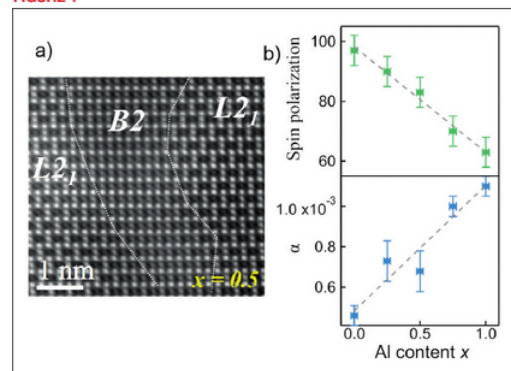
Since the discovery of all-optical control of the magnetization in magnetic layers using laser pulses, many efforts have been made to understand the underlying ultrafast dynamics responsible for the transfer and dissipation of spin angular momentum. Here, tailored $\text{Co}_2\text{MnAl}_x\text{Si}_{1-x}$ epitaxial Heusler films are used to adjust the degree of spin polarization at the Fermi energy P and Gilbert damping α , and to study the impact of these two parameters on the ultrafast demagnetization time τ_M . The latter is shown to be inversely proportional to $1-P$ and consequently to α , suggesting a similarity in the spin momentum dissipation processes involved in these two effects that live on different timescales.

Manipulation of the magnetization on the femtosecond timescale has become an outstanding challenge since the demonstration of sub-picosecond magnetization quenching [1] and magnetization reversal [2]. Despite the theoretical and experimental work that has been reported up to now, the relationship between the spin polarization of electronic states at the Fermi energy (E_F) or the magnetic damping and ultrafast demagnetization excited by femtosecond laser pulses remains unclear. In the present work, we used $\text{Co}_2\text{MnAl}_x\text{Si}_{1-x}$ quaternary Heusler compounds grown by Molecular Beam Epitaxy (MBE) as a playground to test this dependency and get further insights into the relaxation processes involved in this new light-matter interaction.

STRUCTURE AND ELECTRONIC PROPERTIES

The thin films' structure was carefully analyzed using electron and X-ray diffraction together with transmission electron microscopy at the Institut Jean Lamour. Although a B2-type chemical disorder (Mn/Si/Al mixture) is obtained when substituting Si by Al [3], the high crystalline quality and the Heusler structure are preserved for the entire substitution range x , as shown in figure 1-a. This series of compounds was elaborated at the Cassiopée beamline MBE chamber, where the spin polarization P of the electronic states near E_F was measured using *in-situ* spin-resolved photoemission spectroscopy. Figure 1-b shows that controlling the amount of Al substitution in these compounds allows a tuning of the spin polarization from a half-metal magnetic behavior with $P = 100\%$ (spin gap) to a standard magnetic material with $P = 60\%$. Moreover, broadband ferromagnetic resonance measurements shown in figure 1-b demonstrate that the Gilbert damping parameter of these alloys is among the lowest reported for conductive layers [3], and that it is inversely proportional to the measured spin polarization. The high versatility of this class of compounds make them excellent candidates to evaluate the impact of the electronic structure on the ultrafast magnetization dynamics.

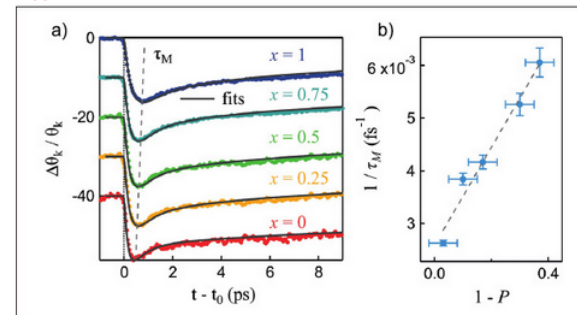
FIGURE 1



ULTRAFAST DYNAMICS MEASUREMENTS

The demagnetization measurements were performed at the Institut Jean Lamour in Nancy, by using a Time-Resolved Magneto-Optical Kerr Effect (TR-MOKE), with a pump-probe geometry. A 35 fs width laser pulse pumps the quenching of the magnetization at time t_0 . The change in magnetization is probed afterward at time t by looking at the change in helicity $\Delta\theta_k$ of a second laser pulse after its passing through the magnetic film (magneto-optical Kerr effect). By adjusting the delay $t-t_0$ between the pump and probe pulses, one can measure the dynamics of the magnetization at a sub-picosecond timescale. Results of ultrafast demagnetization dynamics are presented in figure 2-a, together with fits obtained by using the three-temperature model which describes the energy distribution among electrons, phonons, and spins after laser excitation. The ultra-fast demagnetization time τ_M decreases from 380 fs for Co_2MnSi to 165 fs for Co_2MnAl . The evolution of $1/\tau_M$ as a function of $1-P$ is presented in figure 2-b, where a clear linear variation is observed in these compounds. As the magnetic damping α is inversely proportional to P in our case, this means that $1/\tau_M$ is proportional to α too.

FIGURE 2



DISCUSSION

To the best of our knowledge, the figure 1-b is the first robust demonstration of the link between the magnetic damping and the spin polarization, confirming the theoretical justification of ultra-low damping in half-metal magnets as a consequence of the reduction of spin flip due to the spin gap. The dependency between α and τ_M observed here was a clear opportunity to test the different theoretical explanations proposed in the literature. Several groups [4] proposed that the demagnetization process is linked to the population of minority and majority spin states at E_F , leading to a dependence of the spin-scattering rate proportional to $1-P$ [4]. As this spin scattering rate is linked to the inverse of the demagnetization time, the $\tau_M \sim (1-P)^{-1}$ law was proposed. This law is verified in our samples series and confirms that the spin gap is at the origin of the increase of τ_M . Finally, an inverse relationship between τ_M and α is established in these compounds, which agrees well with models [4,5]. In summary, this work provides a new milestone toward the understanding of the magnetization dynamics at the sub-picosecond timescale, and contributes to pave the way for future efficient devices.



CASSIOPEE BEAMLINE



Associated publication

Engineering $\text{Co}_2\text{MnAl}_x\text{Si}_{1-x}$ Heusler Compounds as a Model System to Correlate Spin Polarization, Intrinsic Gilbert Damping and Ultrafast Demagnetization.



C. Guillemard, W. Zhang, G. Malinowski, C. De Melo, J. Gorchon, S. Petit-Watelot, J. Ghanbaja, S. Mangin, P. Le Fèvre, F. Bertran & S. Andrieu.

Adv. Mater., 32 1908357 (2020).



References

- [1] E. Beaurepaire *et al.*, Phys. Rev. Lett. 76, 4250 (1996).
- [2] C. D. Stanciu *et al.*, Phys. Rev. Lett. 99, 047601 (2007).
- [3] C. Guillemard, PhD thesis, Université de Lorraine (2019).
- [4] A. Mann *et al.*, Phys. Rev. X 2, 041008 (2012).
- [5] B. Koopmans *et al.*, Phys. Rev. Lett. 95, 267207 (2005).



Corresponding authors

Charles Guillemard
ALBA Synchrotron,
Carrer de la Llum 2-26, 08290,
Cerdanyola-del-Vallès,
Barcelona, Spain
cguillemard@cells.es

Stéphane Andrieu
Institut Jean Lamour,
2, allée André Guinier,
54011 Nancy cedex, France
stephane.andrieu@univ-lorraine.fr

Captions

FIGURE 1: a) High resolution transmission electron microscopy micrograph of $\text{Co}_2\text{MnAl}_{0.5}\text{Si}_{1.5}$ showing high structural quality with L2₁ ordered and B2 disordered regions. b) Spin polarization at E_F obtained at Cassiopée beamline and magnetic Gilbert damping α as a function of the substitution range x in $\text{Co}_2\text{MnAl}_x\text{Si}_{1-x}$ compounds.

FIGURE 2: a) Ultrafast demagnetization curves measured by TR-MOKE with the corresponding fit for each composition. b) Evidence of $1/\tau_M$ linear variation with $1-P$.

A model of the hantavirus surface glycoprotein lattice

Hantaviruses are the causative agents of two serious zoonotic diseases for which no treatment is available. They are enveloped viruses covered by an outer lattice formed by two glycoproteins termed Gn and Gc, which are the perfect targets to develop hantavirus countermeasures. We determined the x-ray crystal structures of a heterodimer of Gc and the Gn head, and a homotetramer of the Gn base using data collected from the Proxima beamlines and combined them with a cryoelectron tomography map at 11 Å resolution to obtain a detailed model of the surface glycoprotein shell. We also revealed a built-in mechanism controlling Gc insertion into cellular membranes for fusion. These results pave the way for immunogen design to protect against pathogenic hantaviruses.

Hantaviruses are rodent-borne viruses distributed worldwide. They are classified as Old World and New World hantaviruses depending on their geographical distribution and natural reservoirs [1]. They are transmitted to humans via inhalation of aerosols contaminated with infected rodent excreta, causing two different severe diseases; haemorrhagic fever with renal syndrome (HFRS) and hantavirus pulmonary syndrome (HPS) with fatality rates of up to 12% (HFRS) and 40% (HPS). Despite the severity of these diseases, no efficient treatment is available.

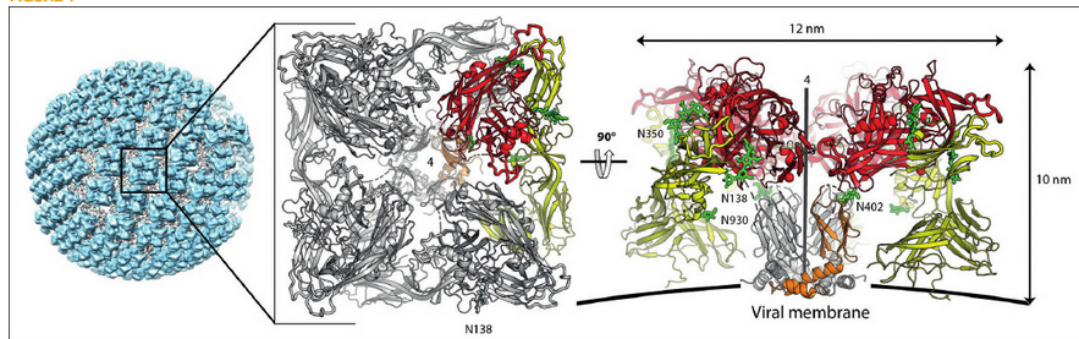
The *Hantaviridae* constitute one of 12 families of the order *Bunyvirales*. The viral genome is composed of three segments of ssRNA of negative-polarity. The medium segment encodes a polyprotein precursor that is further processed in the endoplasmic reticulum to yield two glycoproteins, termed Gn and Gc. Gn interacts co-translationally with the membrane fusion protein Gc to form a metastable Gn/Gc heterodimer [2]. The protomers further associate into (Gn/Gc)₄ tetrameric spikes that are transported to the site of particle morphogenesis, where lateral interaction between adjacent spikes induce the membrane curvature required for budding new virions. Hantavirus particles are internalized into target cells via receptor-mediated endocytosis, and the outer lattice then reacts to the acidic pH of the endosomes and drive the fusion of viral and cellular membranes through a conformational change of Gc.

In line with their importance, both glycoproteins have been widely studied by us and others, and the x-ray structures of the isolated Gn “head” (the N-terminal two-thirds of the ectodomain, Gn^H) [3] and ectodomain of Gc reported [4]. The structures of the latter showed to feature the characteristic β sheet-rich domain observed in the class II fusion proteins of flaviviruses, alphaviruses, phleboviruses, and rubella virus, suggesting an evolutionary link between otherwise different viral families. The organization of the outer lattice has been studied at low resolution by electron microscopy [5]. Despite these advances, the actual organization of the spike and the molecular interactions between Gn and Gc have remained elusive.

RESULTS

Thanks to data collected in Proxima 1 and 2 beamlines, we have obtained the X-ray structures of the metastable pre-fusion Gn^H/Gc complex of Andes (ANDV) and Maporal (MAPV, closely related to ANDV) viruses to 3.2 and 2.2 Å resolution, respectively. We have also obtained the X-ray structure of the Gn “base” (the missing C-terminal third of Gn, Gn^B), at 1.9 Å resolution and showed that it forms a tight tetramer. We have fitted these structures into a cryo-electron tomography map of Tula virus (TULV, a non-pathogenic Old world hantavirus) refined to 11.4 Å resolution. The fitting confirmed that the heterodimeric and homotetrameric conformations captured in the crystals correspond to their active form in the spikes of infectious particles, and provided a complete model for the surface glycoprotein lattice (Fig. 1). This model provided a framework to understand an accumulating body of data on hantavirus biology. For example, it revealed that the conserved N-linked glycans are buried in the spike, explaining why they remain high-mannose in the released particles, and supporting the hypothesis that the tetrameric spikes form early in the ER and are transported as such to the Golgi apparatus. Moreover, the model paves the way for the development of novel immunogens by providing ways to design stabilized versions of the heterodimer and the spikes. We provided a proof of principle that such stabilization is possible by designing disulfide bonds linking both subunits. Also, using data collected in the Proxima beamlines, we have also obtained the structure of the post-fusion form of Gc from ANDV and MAPV at 2.4 and 2.7 Å resolution, respectively. Unlike other class-II fusion proteins studied so far, the tip of Gc domain II, where a critical membrane-interacting region is located, adopts an alternative conformation that reduces surface hydrophobicity, preventing the interaction with membranes in the presence of Gn. Last but not least, the structure of the heterodimer Gn/Gc revealed a strong similarity with the fusion machinery E1/E2 of the alphavirus, suggesting a common origin and therefore providing unanticipated evolutionary links.

FIGURE 1



PROXIMA-1 & PROXIMA-2A BEAMLINES

Associated publication

The Hantavirus Surface Glycoprotein Lattice and Its Fusion Control Mechanism.



A. Serris, R. Stass, E. A. Bignon, N. A., Muena, J. C. Manuguerra, R. K. Jangra, S. Li, K. Chandran, N. D. Tischler, J. T. Huiskonen, F. A. Rey, P. Guardado-Calvo.

Cell, 183(2): 442 (2020).

References

- [1] C. B. Jonsson *et al.*, Clin Microbiol Rev. 23, 412 (2010).
- [2] P. Guardado-Calvo & F.A. Rey, Adv Virus Res, 98, 83 (2017).
- [3] I. Rissanen *et al.*, J Virol, 91(21) (2017).
- [4] P. Guardado-Calvo *et al.*, PLoS Pathog, 12(10): p. e1005813 (2016).
- [5] S. Li *et al.*, Cell Rep, 15, 959 (2016).



Corresponding authors

Felix A. Rey & Pablo Guardado-Calvo
Institut Pasteur, Structural Virology Unit, and CNRS UMR 3569
Paris, France
rey@pasteur.fr
guardado@pasteur.fr

Caption

FIGURE 1: The structure of the hantavirus spike. Reconstruction of a Tula virus particle at 11 Å resolution. The resulting surface protein lattice is shown in cyan and the viral membrane in gray. The middle and right panels show top and side views of a single spike, with one of the four protomers colored in red (Gn^H), orange (Gn^B) and yellow (Gc) and the sugar residues in green.

Short- and long-term effect of radiation damage in cotton paper

The analysis of cultural heritage artefacts with ionizing radiation has rapidly increased in popularity over the last decades - in particular at synchrotron sources - leading to many fascinating new discoveries. However, the damage inflicted to the materials under study during the irradiation is still largely unknown. Organic samples, such as paper, are especially vulnerable to degradation by X-rays. In this work we quantify the radiation damage on a molecular level and show that the chemical reactions triggered promote cellulose degradation and continue to alter the material for several months after the irradiation took place.

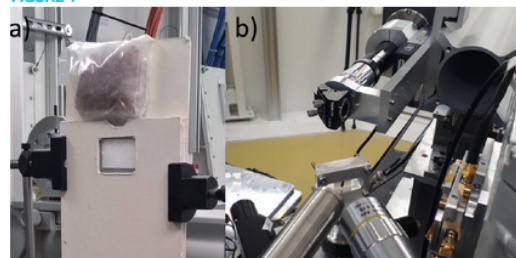
Paper artefacts are an important part of our cultural heritage. Aside from drawings and other paper-based artworks, archival and library material such as private letters and public documents also give us a unique insight into the written heritage of past generations. A large part of this immense cultural heritage treasure is still hidden from the public at large, but is of enormous importance to historians and codicologists. Special care is needed for their conservation as they can easily be destroyed by fire, water damage or attacks from microorganisms and insects. While the composition of paper is complex and varied considerably over the course of history, its basic structural level consists of a network of plant fibers made of cellulose. Cellulose is the most abundant naturally occurring macromolecule on earth. It is a polysaccharide with the chemical formula $(C_6H_{10}O_5)_n$. To understand the fundamental radiochemistry of paper, in this research we used a simple paper (Whatman no. 1), made of cotton linters, which is almost exclusively cellulose (99%).

IRRADIATION

The use of ionizing radiation, and especially synchrotron X-ray, for the analysis of paper artefacts has increased rapidly over the last decades [1]. For example, the use of X-ray fluorescence imaging allows scientists to reveal blacked-out ink writings, thus unearthing information that was beyond reach for centuries [2]. However, when the X-ray photons interact with cellulose, they can break chemical bonds and depolymerize the molecules. This initiates further chemical degradation that can continue on larger timescales than the irradiation duration.

To recreate conditions as close as possible to a real synchrotron experiment, in this study we used the PUMA beamline (Figure 1). The paper samples were irradiated with different X-ray doses using the macro beam ($1 \times 2 \text{ cm}^2$) and with a photon energy of 7.22keV (wavelength 1.7 Å). The effect of paper moisture content was investigated using different silica gels to maintain three different relative humidity levels during irradiation (Figure 1a).

FIGURE 1



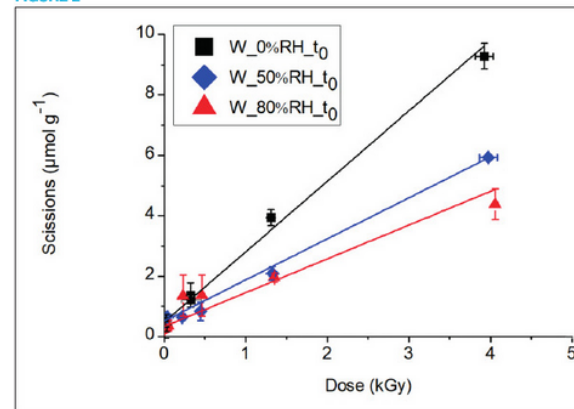
MONITORING THE RADIATION DAMAGE ON THE MOLECULAR SCALE

When evaluating radiation damage, it is important to look beyond macro-scale observations, such as a color change for instance, and focus on the changes incurred in the molecular structure of the material, due to the interaction with photons. To characterize the depolymerization, indicator of hydrolytic scissions of cellulose, and hence molecular length shortening and fiber damage, size-exclusion chromatography (SEC-MALS-DR1) was used. High-performance liquid chromatography (HPLC-FLD-DAD) allowed the quantification of hydroxyl free radicals, which are indicators of the cellulose auto-oxidation phenomena. This approach was complemented by macro-scale observations such as UV luminescence, spectrometry and photography.

SHORT AND LONG TIME SCALES

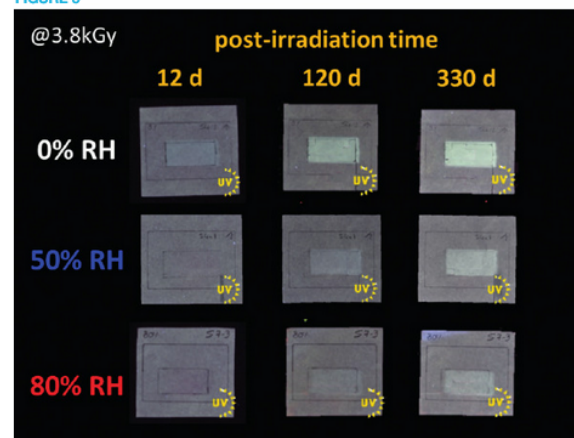
Our analysis showed that chemical damage happened on the molecular scale during the irradiation, starting from a relatively low dose of 21 Gy. It was observed that the higher the dose of SR-X radiation absorbed by the paper, the greater the depolymerization and the higher the concentration of hydroxyl free radicals. This behavior can be seen in Figure 2, which shows glycosidic scissions as a function of the dose for paper samples irradiated at different relative humidity conditions. The impact of humidity is unmistakable; there is less damage in humid paper than in dry paper.

FIGURE 2



To monitor irradiation changes over longer time scales, the samples were stored under controlled thermohygrometric conditions and the physio-chemical changes were studied over a period of two years. We could show that the UV-luminescence signal and the yellowing of the paper (Figure 3), as well as the depolymerization and the auto-oxidation of cellulose continued increasing over time, indicating that the chemical degradation reactions were still taking place several months after the irradiation. This finding is important for conservators, as it shows that a simple check for macroscopic changes after the irradiation does not preclude potential future harm to the material. Our results quantify the impact of X-rays radiation to paper samples at both the molecular and macroscopic scale for the first time. Further work is in progress to better understand the effect of natural aging and the impact of additives (sizing, inks, fillers) that are part of real artefacts.

FIGURE 3



PUMA BEAMLINE

Associated publication

Short and long term effects of X-ray synchrotron radiation on cotton paper.

A. Gimat, S. Schöder, M. Thoury, M. Missori, S. Paris-Lacombe, A.-L. Dupont.

Biomacromolecules, 21, 2795(2020).

References

- [1] L. Bertrand *et al.*, Physics Reports 519, 51 (2012).
- [2] E. Pouyet *et al.*, Analytica Chimica Acta 982, 20 (2017).

Corresponding author

Alice Gimat
Centre de recherche sur la conservation des collections
CRCC
USR3224 CRC
Muséum national d'histoire naturelle
36 rue Geoffroy-Saint-Hilaire - CP 21
75005 Paris
alice.gimat@mnhn.fr

Captions

FIGURE 1: Experiments on PUMA beamline: a) paper inside a plastic bag with silica gel to maintain a stable relative humidity during irradiation with the macro beam and b) paper irradiation with the micro beam.

FIGURE 2: Glycosidic scissions concentration (S) as a function of SR-X dose. The irradiation took place at different relative humidity levels (0%, 50% and 80%) at room temperature.

FIGURE 3: UV luminescence image of Whatman no. 1 paper samples irradiated on PUMA beamline at 3.8 kGy at various relative humidity levels (0%, 50% and 80%) at room temperature. Luminescence appears in the irradiated area ($1 \times 2 \text{ cm}^2$) gradually and differently depending on the relative humidity.

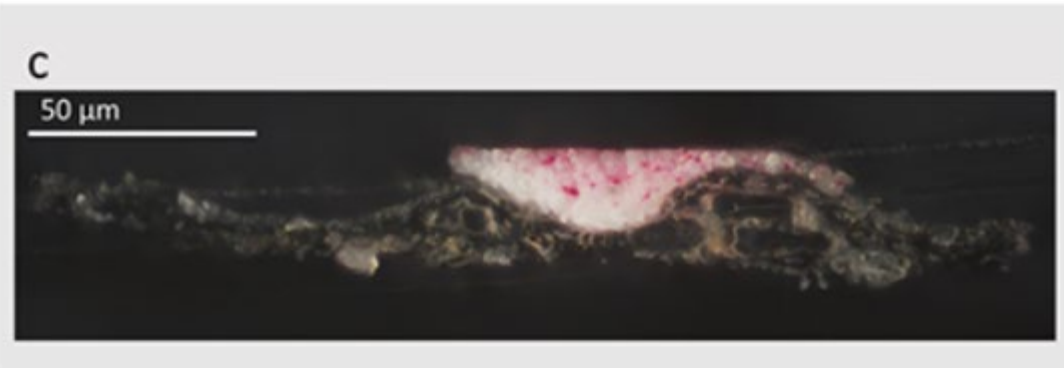
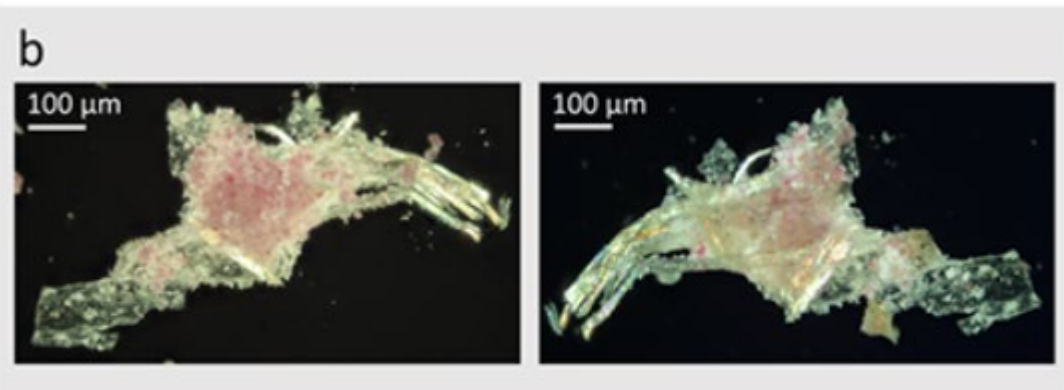


Figure 1:

a) *L'Arlésienne* (portrait of Madame Ginoux) from Van Gogh, 1890. Kröller-Müller Museum

b) fragment extracted from the painting

c) thin section of the fragment.

Atelier microscope

Travail par équipe : 2

Transformez votre smartphone en microscope

Atelier microscope

Travail par équipe : 2

Transformez votre smartphone en microscope

Testez effet de la taille de la goutte

Atelier microscope

Travail par équipe : 2

Transformez votre smartphone en microscope

Testez effet de la taille de la goutte

Inventez un atelier pour des élèves

Contexte

Stand fête de la science

Activité à la maison

Activité en classe pédagogique

Activité en classe brise glace

....

